The Role of Biaxial Loading on Smooth Muscle Contractility in the Nulliparous Murine Cervix

Conway, Cassandra K.

Department of Biomedical Engineering, Tulane University

6823 St. Charles Ave, New Orleans, LA 70118 USA

cconway2@tulane.edu

Varghese, Asha

Obstetrics and Gynecology and Green Center for Reproductive Sciences

University of Texas Southwestern Medical Center

Dallas, TX 75390 USA

Asha.Varghese@UTSouthwestern.edu

Mahendroo, Mala

Obstetrics and Gynecology and Green Center for Reproductive Sciences

University of Texas Southwestern Medical Center

Dallas, TX 75390 USA

Mala.Mahendroo@utsouthwestern.edu

Miller, Kristin S.*

Department of Biomedical Engineering, Tulane University

6823 St. Charles Ave, New Orleans, LA 70118 USA

504 988-9324

kmille11@tulane.edu

Abstract

Throughout the estrus cycle, the extracellular matrix (ECM) and cervical smooth muscle cells (cSMC) coordinate to accomplish normal physiologic function in the non-pregnant cervix. While previous uniaxial experiments provide fundamental knowledge about cervical contractility and biomechanics, the specimen preparation is disruptive to native organ geometry and does not permit simultaneous assessment of circumferential and axial properties. Thus, a need remains to investigate cervical contractility and passive biomechanics within physiologic multiaxial loading. Biaxial inflation-extension experiments overcome these limitations by preserving geometry, ECM-cell interactions, and multiaxially loading the cervix. Utilizing *in vivo* pressure measurements and inflation-extension testing, this study presented methodology and examined maximum biaxial contractility and biomechanics in the nulliparous murine cervix. The study showed that increased pressure resulted in decreased contractile potential in the circumferential direction, however, axial contractility remained unaffected. Additionally, total change in axial stress (ΔT_{zz}) increased significantly (*p<0.05)* compared to circumferential stress ($\Delta T_{\theta\theta}$) with maximum contraction. However, passive stiffness was significantly greater (*p<0.01)* in the circumferential direction. Overall, axial cSMC may have a critical function in maintaining cervical homeostasis during normal function. Potentially, a loss of axial contractility in the cervix during pregnancy may result in maladaptive remodeling such as cervical insufficiency.

Keywords: Cervix, Reproductive Health, Contractility, Biomechanics

Introduction

The coordination of smooth muscle cells (SMC) and extracellular matrix (ECM) components impart function to the female reproductive system[22]. Altered contractility and passive mechanical properties, in response to mechanical loading and hormonal signaling, bestow the reproductive system with the ability to undergo dramatic changes in geometry and function during physiological processes, such as pregnancy[4, 13, 15, 16, 24-26, 33, 39]. Determining contractile and passive biomechanical properties of the female reproductive organs could provide crucial information about physiologic reproductive function. Specifically, the cervix functions to protect the uterine cavity from external factors, facilitate fertilization, and dilate to allow for the passage of menstrual contents in the non-pregnant state through regular phasic contractions[13, 22]. However, the role and behavior of cervical SMC (cSMC) in reproductive function is contradictory and remains poorly understood[12, 51, 52].

While uterine contractility and passive mechanical properties during the estrous/menstrual cycle and pregnancy garnered focus in prior research, the demonstration that SMCs are present in the human and rodent cervix warrants further understanding of their role in the non-pregnant state[6, 10, 14, 27, 34, 35, 40, 41, 43, 49, 57]. In 1947, Danforth described the human cervix as a primarily collagenous organ with limited SMC and contractile ability[12]. The research proposed a significant active SMC contribution from the uterus and a passive role of the cervix during pregnancy and labor[12]. However, recent research emphasizes the independent role of cervical contractile function and mechanical behavior in the non-pregnant and pregnant states[10, 13, 16, 22, 51, 52]. Prior work, to a limited extent, investigated *in vitro* cervical contractility utilizing strips, rings, or individual cSMCs

in human[51, 52] and rodent models[13, 16, 22]. Although the experimental methods provided fundamental information about the contractile behavior of the cervix, the experiments require disruptive specimen preparation techniques and assess circumferential and axial properties independently[13, 16, 22, 25, 38, 56]. The cervix is anisotropic and loaded multiaxially within the body, thus, there is a need to utilize testing methods that retain cervical geometry, native ECM-cSMC interactions, and simultaneously quantify circumferential and axial contractility within a physiologic loading environment[9, 10, 19, 54].

Biaxial inflation-extension testing overcomes limitations imposed by uniaxial configurations by simultaneously loading tissues circumferentially via pressurizing the organ within a physiologic range and longitudinally by axially extending the organ[21]. Previously, biaxial inflation-extension testing quantified mechanical properties of vasculature[5, 19-21, 44], the GI tract[45, 46], and reproductive organs[2, 9, 10, 42, 54]. Additionally, research determined contractile behavior in vasculature[30, 36, 58] and the vagina[9] utilizing inflation-extension testing. However, there is a need to describe the *in vivo* cervical loading environment to permit assessment of contractility and passive biomechanics within a physiologically relevant range *ex vivo.* Therefore, this study seeks to introduce methods to determine the *in vivo* cervical pressure environment and utilize the information to design a protocol to determine the biaxial maximum contractility and passive mechanics of the murine cervix.

Materials and Methods

Animal Care

Mechanical testing experiments herein were conducted on a total of *n=10* nulliparous CD-1 female mice aged 8-12 weeks (Charles River, Houston, TX). The Tulane University Institutional Animal Care and Use Committee (IACUC) approved of care and the conducted experiments. Immunofluorescence experiments were conducted on a total of *n=2* nulliparous C57Bl6/SvEv female mice aged 12-24 weeks with approval from the University of Texas Southwestern IACUC. These mice were bred and maintained within a breeder colony at The University of Texas Southwestern Medical Center (Dallas, TX). Mice were provided a normal chow diet and housed in a 12-hour light/dark cycle. All mice were cycle matched at estrus via visual determination[7].

In Vivo Pressure Measurements

Attempting to recapitulate the key aspects of the *in vivo* loading environment during mechanical testing can provide important information about the mechanical behavior and contractility at an estimated physiologic state. Therefore, transcervical pressure measurements were taken from (*n = 5)* mice at estrus to determine the estimated loading environment for the murine cervix during mechanical testing **(Fig. 1)**[43]. A 2F Millar Mikro-tip® Catheter (ADInstruments, Colorado, USA) was connected to ADInstruments Bridge Amplifier and PowerLab (ADInstruments, Colorado, USA) and allowed to equilibrate in a water bath filled with physiologic saline at 37°C for 30 minutes. Utilizing a Y connection tube, the catheter was calibrated with a pressure gauge after the 30-minute equilibration.

Mice were anesthetized with 1%-1.5% isoflurane mixed with 100% O_2 and placed on a heating pad[43]. Using blunt forceps and a disposable plastic tube acting as a speculum, the vagina was gently spread laterally. Next, a directed light source aligned down the plastic tube allowed for the cervical centered within the vaginal fornix to be visualized.

Following, the pressure catheter was inserted into the cervical canal. Appropriate placement of the catheter was confirmed with a marking approximately 6 mm from the probe based on the length of the vagina from prior studies[9, 42], an increase in pressure[43], and phasic contractions[13, 22]. Upon confirmation of appropriate placement, the catheter equilibrated for 5 minutes followed by 5 minutes of recorded data on LabChart Pro software (ADInstruments, Colorado, USA). Recorded data measured baseline pressure, pressure with contraction, and frequency of contraction (**Fig. 1**). After data recording, the catheter was removed and soaked in Terg-A-Zyme®, an enzymatic cleaning solution, for 15 minutes. Between each procedure the catheter was cleaned with the enzymatic cleaning solution, equilibrated for 30 minutes, and calibrated. Mice were monitored and allowed to recover in a separate clean cage before returned to littermates.

Specimen Preparation

A total of (*n*=10) CD-1 female mice cycle matched at estrus were utilized for dose response and contractility protocols. Wherein, recovered mice from the *in vivo* pressure procedure (*n=5*) were assigned to the dose response study at the following estrus phase. Additionally, a separate cohort of CD-1 mice (*n=5*) were utilized for the maximum contractility and passive mechanics protocol[7]. The following sample preparation techniques applied to both protocols listed below. All mice were euthanatized via guillotine to preserve SMC viability[9]. The reproductive systems were excised from mice immediately and submersed in 4°C Hanks Balanced Saline Solution (HBSS). The cervical complex was isolated from the reproductive tract by singular cuts superior to the distal vaginal and inferior to the uterine body **(Supplemental Figure 1)**. Next, the cervix was cannulated with 6-0 silk suture within a biaxial inflation-extension device (Danish

MyoTechnologies, Aarhus, Denmark). HBSS was replaced with 37°C Kreb's Ringer Buffer (Kreb's Buffer) aerated with 95% O_2 and 5% CO_2.

During excision, the reproductive organs retract from the original position following dislocation of the pubic synthesis and subsequent removal of fascial tetherings[10, 42, 54]. Due to the retraction, the cervix was extended to an estimated unloaded length in which the organ was neither in tension nor buckled and pressurized with a tare pressure of P= 3.0 mmHg to prevent collapse of the organ at P= 0 mmHg[2, 10, 42]. Unloaded length and unloaded outer diameter at the tare pressure was recorded with digital calipers and a Nikon Eclipse TS100 inverted microscope (Nikon®, Melville, NY, U.S.A.), respectively. Utilizing the mean *in vivo* baseline pressure measurements from the *in vivo* pressure measurement experiments (**Fig. 1**), the mean physiological pressure for mechanical testing protocols was determined as P= 9.0 mmHg. To maintain SMC viability, the maximum pressure extended to one standard deviation below the mean maximum contractile pressure (P= 22.0±4.0 mmHg). Cervices were preconditioned circumferentially at the unloaded length for 5 cycles of increasing and decreasing pressure (P= 0-18 mmHg). Following, an estimated physiological (EP) length was determined first by using the measured retraction following dissection, followed by leveraging the theoretical assumption that axial force will be maintained with increasing pressure over the physiologic range to preserve energy as described previously[50]. Additional circumferential preconditioning (P= 0-18 mmHg) was performed at the EP length for 5 cycles and axial preconditioning performed by cyclically stretching cervices axially ±1% the EP length at 1/3 max pressure (P= 6.0 mmHg)[5, 10]. Following preconditioning, the unloaded length was re-determined[9]. To acclimate cSMCs to potassium chloride (KCl), the cervical complex

was pressurized to the mean physiologic pressure (P= 9.0 mmHg) at the unloaded length, axially extended until the axial force held constant at 0mN, and dosed with 20mM KCl for 5 minutes[9, 36]. Following, the bath was replaced with fresh Kreb's buffer and the cervix elongated to the EP length. The cervix at the EP length and mean physiologic pressure equilibrated for 10 minutes[10, 42].

Dose Response

To determine the optimal dose of the agonist potassium chloride (KCl) to induce maximum contraction, an isometric-isobaric dose response protocol was performed at the EP length and the mean physiologic pressure (P = 9.0 mmHg) for the first cohort of animals (*n=5*). Following the equilibration period, tissues were subjected to increasing concentrations of KCl (4.7-100mM)[8] at the EP length and mean physiologic pressure. Between each dosing, the cervix was washed and submerged in fresh Kreb's solution and equilibrated for 5 minutes. Circumferential and axial contractions were measured via diameter changes tracked at the mid-cervix and changes in measured axial force with a camera and force transducer, respectively (**Fig. 2**).

Biaxial Contractility and Passive Mechanics

Maximum Contractility

Utilizing the second cohort of mice (*n*=5), cervices underwent a contractility protocol with nine combinations of physiologic lengths and pressures to assess the role of circumferential and axial loading on contractility following the equilibration period [36] **(Fig. 3)**. Each combination randomized the length (the EP length and ±1% EP length) and pressure (mean ± standard deviation of the physiologic pressure; P= 9.0±3.0 mmHg).

Data was recorded for 5 minutes after 20mM KCl dosing followed by a resting period for 5 minutes after buffer replacement or after pressure and axial length change[36]. Then, the cervices were returned to the unloaded geometry and B-mode ultrasound images (Vevo2100; 40MHz transducer) of cervical thickness were taken at the unloaded state[9, 10].

Passive Mechanics

Returned to the EP length of the maximum contractility experiment, cervices were bathed in calcium-free Kreb's and dosed with 2mM egtazic acid (EGTA) for 30 minutes to remove active SMC contribution. Abiding by the steps outlined in *Specimen Preparation*, passive unloaded geometry measurements, unloaded circumferential preconditioning, determination of the passive EP length, and circumferential and axial preconditioning were performed followed by 10 minutes of equilibration. Three cycles of a pressure-inflation protocol were performed at the EP length and ±1% the EP length from P= 0-18 mmHg[10, 42, 54]. Following, axial force-elongation protocols ±1% EP length over a range of pressures (P= 3, 6, 12, and 18 mmHg) were performed[10, 42, 54]. The cervix was returned to the unloaded geometry and the thickness recorded with ultrasound.

Immunofluorescence

Transverse and longitudinal sections (5μm) of the cervix at estrus (n=2) were deparaffinized, blocked, and co-stained with primary and secondary antibodies. Markers targeted included αSMA (Anti-Mouse 1:300, Monoclonal Anti-Actin, α-Smooth Muscle, A2547, Sigma-Aldrich) and Vimentin (Anti-Rabbit 1:250, Recombinant Anti-Vimentin antibody [EPR3776]-Cytoskeleton Marker, ab92547, Abcam). After overnight primary

antibody incubation at 4ºC, the slides were washed and incubated with secondary antibody (Goat anti-Rabbit 1:500 (H+L) Cross-Adsorbed Secondary Antibody, Alexa Fluor 488,A-11008, and Goat anti-Mouse 1:500 (H+L) Highly Cross-Adsorbed Secondary Antibody, Alexa Fluor 546, A-11030, Invitrogen-ThermoFisher Scientific) for 30 minutes at room temperature. After PBS washes, slides were mounted with ProLong™ Gold Antifade Mountant with DAPI (P36935, ThermoFisher Scientific) and viewed on a Zeiss LSM-880 Confocal Microscope (Zeiss International, New York, USA) at 20X magnification. For each transverse and longitudinal tissue section, both the sub-epithelial and mid-stromal regions were imaged in at least four locations at 20X and 40X.

αSMA and Vim positive area fractions for the mid-stroma and subepithelium in the transverse and longitudinal sections were calculated utilizing ImageJ (National Institutes of Health, Bethesda, MD, U.S.A.) and GIMP, an open source image manipulation program. Images from the red (αSMA) and green (Vim) color channels were inverted and converted to gray scale in ImageJ. The inverted images were opened in GIMP and a histogram tool within the software was adjusted to represent the range of intensities of the positive cell staining. The area fraction was determined as the number of pixels within the boundaries of the threshold divided by the total number of pixels in the image.

Data Analysis

Thickness, Area, and Volume Calculation

Utilizing ultrasound images and ImageJ (National Institutes of Health, Bethesda, MD, U.S.A.) software, the inner canal and outer circumference excluding the vaginal fornix were traced and lines drawn between the inner and outer perimeters were used to

240 measure thickness. To determine cross sectional area and volume, cervical geometry
241 was simplified to a hollow cylinder. Applying unloaded geometry (length, diameter, and
242 thickness), cross-sectional area (A), and volume (V) were determined using the following
243 equations **(Eq. 1,2)**:

244 $$A = \pi(R_o^2 - R_i^2) \quad \textbf{(1)}$$

245 $$V=\pi(R_o^2\text{-}R_i^2)\mathrm{L}\ , \quad \textbf{(2)}$$

246 where R_o is the undeformed outer radii, R_i the undeformed inner radii, and L the unloaded
247 length.

248 Circumferential stretch (λ_θ) and axial stretch (λ_z) were determined by **(Eq. 3, 4)**[19]:

249 $$\lambda_\theta = r_{mid}/R_{mid} \quad \textbf{(3)}$$

250 and

251 $$\lambda_z = {}^{l}/_{L} \quad \textbf{(4)}$$

252 wherein $r_{mid} = {}^{r_o - r_i}/_2$ is the deformed mid-wall radius, $R_{mid} = {}^{R_o - R_i}/_2$ is the
253 unloaded mid-wall radius, and l is the deformed length.

254 *Contractility*

255 Circumferential and axial contraction were determined via changes in diameter and
256 axial force, respectively **(Fig. 4)**. Additionally, circumferential ($T_{\theta\theta}$) and axial (T_{zz}) 1st
257 Piola-Kirchhoff stress with maximum contraction were determined **(Eq. 5, 6)**[28, 30].

258 $$T_{\theta\theta} = \frac{Pr_i}{\lambda_\theta(r_o - r_i)}, \quad \textbf{(5)}$$

$$T_{zz} = \frac{F_t}{\lambda_z \pi (r_o^2 - r_i^2)} + \frac{P r_i^2}{\lambda_z (r_o - r_i)(r_o + r_i)}, \quad \textbf{(6)}$$

Wherein P is intraluminal pressure, , $r_i = \sqrt{r_o^2 - \frac{A}{\pi \lambda_z}}$ is the deformed inner radius, r_o is the deformed outer radius, and F_t is the force from the axial force transducer[10, 19, 30]. Contribution of the active SMC to the change in stress with contraction (ΔT) was calculated by subtracting the relaxed or passive state stress ($T_{passive}$) from the contracted stress ($T_{contracted}$) at matching axial-extensions and pressures **(Eq. 7, 8)**[1, 9, 30, 36, 58]:

$$\Delta T_{\theta\theta} = T_{\theta\theta}^{contracted} - T_{\theta\theta}^{passive} \quad \textbf{(6)}$$

$$\Delta T_{zz} = T_{zz}^{contracted} - T_{zz}^{passive} \quad \textbf{(7)}$$

Material Stiffness

Material stiffness in the circumferential and axial loading directions were determined by calculating the slope of the stress-stretch curves at a physiologic range of pressures (P= 9.0±3.0 mmHg).

Statistics

Paired t-tests were utilized to determine differences between *in vivo* baseline and maximum pressure and differences in passive and active geometry. One-way ANOVA with respect to dose determined changes in circumferential and axial contractility. Two-way ANOVAs (axial-stretch, pressure) were utilized to determine differences in circumferential and axial contractility. Further, a two-way ANOVA with respect to axial-stretch and loading direction was used to determine differences in circumferential and axial material stiffness. Posthoc t-tests with Bonferroni corrections were utilized when appropriate ($p<0.05/2$).

Results

All results presented herein are represented as mean±SEM apart from the *in vivo* data which is presented as the mean±sd. *In vivo* pressure data are represented as mean±sd to provide a larger margin of error to better capture the contractile response within the *in vivo* pressure range.

In vivo Pressure and Dose Response

In vivo transcervical pressure measurements at estrus revealed an average *in vivo* baseline pressure of 9.00±3.00 mmHg (mean±sd), maximum contractile pressure of 22.0±4.00 mmHg (mean±sd), and a frequency of one contraction per 23.5±5.64 seconds (mean±sd) **(Fig. 1)**. Paired t-tests confirmed a significant increase ($p<0.01$) in cervical pressure from baseline to maximum amplitude with contraction *in vivo.*

Dose response curves of KCl at the EP length and mean physiologic pressure identified 20mM as the optimal dose to induce maximum contraction **(Fig. 2).** Axial force with contraction with dose increased significantly ($p<0.05$) at 20mM compared to all doses followed by a plateau of axial force during contraction at higher doses (30mM-100mM) of KCl. Change in diameter with contraction decreased maximally at 20mM-100mM compared to 4.7mM, 10 mM KCl, and 60mM dosing. Further, phasic behavior abated with increasing dose (30-100 mM) of KCl and the axial force and outer diameter transitioned into a tonic contractile behavior **(Fig. 2).**

Geometry

Passive physiologic diameter (*p<0.05)*, EP length *(p<0.01)*, and volume *(p<0.005)* significantly increased compared to active geometry. However, thickness did not differ significantly between the active and passive state **(Fig. 5)**.

Biaxial Contractility

Induction of maximum contraction with 20mM KCl induced phasic contractions that resulted in a decrease in diameter and increase in axial force **(Fig**. **3, 6).** Additionally, all samples contracted spontaneously without an agonist introduced to the bath as seen previously in nulliparous mice at estrus[22]. Two-Way ANOVA (axial-stretch, pressure) did not detect differences with axial-extension (*p=0.60)* or between interactions (*p=0.90*). However, ANOVA detected significance (*p<0.001)* with respect to pressure for circumferential contractility. Posthoc t-tests with Bonferroni corrections (p<0.05/2) determined significant effects on change in outer diameter with increased pressure (*p<0.001*). Specifically, total change in diameter at high pressure (P= 12 mmHg) diminished significantly (*p<0.001*) compared to total change in diameter at low pressure (P=6 mmHg) **(Fig. 6)**. However, Two-Way ANOVAs (axial-stretch and pressure) determined no significant differences with axial-extension (*p=0.40)*, pressure *(p=1.00)*, or interactions (*p=1.00*) with the change in axial force with maximum contraction. Additionally, frequency and wavelength of contractions during the maximum contractility protocol did not differ with alterations to pressure (*p=0.90)*, axial-stretch (*p=0.20),* or interactions (*p=0.95)* (**Fig. 6)**.

The contracted SMCs and passive ECM contribute to the overall cervical biomechanical properties, including wall stress (force over oriented area). Subtracting the passive stresses from the active contractile stresses at matching pressures and axial-

stretches quantifies the contribution of the active SMC during contraction[30, 36]. Maximum contraction induced a decrease in the change in circumferential stress ($\Delta T_{\theta\theta}$) and increase in axial stress (ΔT_{zz}) at all pressures and axial-stretches **(Fig. 7).** Two-Way ANOVA (axial-stretch, pressure) did not detect significant differences for $\Delta T_{\theta\theta}$ or ΔT_{zz} with change of pressure or axial-stretch. Total ΔT_{zz} increased significantly with maximum contraction compared to $\Delta T_{\theta\theta}$ (*p<0.05)* at the EP length and pressure **(Fig. 7)**.

Biaxial Passive Mechanics

Passive material stiffness calculated from the slope of stress-stretch curves over a range of physiologic pressures (P= 9.0±3.0 mmHg) was significantly greater (*p<0.01)* in the circumferential direction compared to the axial direction **(Fig. 7)**[9, 47]. Circumferential stiffness at the physiologic length measured 327± 142 kPa and axial stiffness measured 136 ± 51.2 kPa **(Fig. 7)**. Further, no significant differences in circumferential or axial stress were identified with axial-extension **(Supplemental Figure 2)**.

Immunofluorescence

Immunofluorescence of transverse and longitudinal cervical sections identified fibroblast ($\alpha SMA^-, Vim^+$) and cSMC (αSMA^+, Vim^-) cell types within the stroma and the stromal region adjacent to the epithelia, termed the sub-epithelial layer. Within the mid-stroma, cSMC (αSMA^+, Vim^-) and fibroblast ($\alpha SMA^-, Vim^+$) populations are identified **(Fig. 8).** Within the transverse sections, αSMA^+ cells comprised 9.49±3.69% of the area and Vim^+ cells filled 14.2±0.94% of the area. Longitudinal section area fractions calculated 11.2±3.30% αSMA^+ cells and 17.7±3.80% Vim^+ cells. In contrast, the sub-epithelial layer contains only fibroblast ($\alpha SMA^-, Vim^+$) cells in the estrus cervix with an area fractions of

16.45±3.45% and 13.4±2.07% in the circumferential and axial directions, respectively **(Fig. 8).** Interestingly, a subpopulation of (αSMA^{+} ,Vim^{+}) cells reside within the mid-stroma.

Discussion

This study, for the first time, presented methods to determine biaxial maximum contractility within a physiologic loading environment in the murine cervix utilizing inflation-extension techniques. Additionally, transcervical pressure catheter experiments described the *in vivo* baseline pressure and contractile amplitude and frequency in the murine cervix.

Historically, research considered the cervix as an extension of the uterus with minimal or no independent contractile ability[12]. However, recent studies emphasized the importance and individual nature of the cSMC microstructure and behavior compared to the other reproductive organs[13, 16, 22, 51, 52]. Further, Vink *et al.* described an altered contractile response of cSMC with respect to ECM stiffness suggesting that mechanical loading may dictate cervical contractile behavior[51]. While prior work investigated the uniaxial contractile behavior of the cervix, the methods did not preserve the native ECM-cell interactions and did not account for multiaxial loading of the cervix *in vivo*[13, 16, 22]. Biaxial inflation-extension active and passive mechanical testing methods well-established in vasculature[8, 19, 28, 30, 36, 58] provide a blueprint for determining protocols to assess biaxial contractility in hollow organs, such as the cervix. Through adapting maximum contractility protocols from vasculature[36] and the vagina[9], this study fulfills a need to determine experimental procedures to describe the multiaxial contractility of the cervix within a physiologically relevant mechanical loading environment.

Herein, we described biaxial maximum contractility and passive biomechanics within a physiologic loading environment motivated by *in vivo* pressure measurements of the murine cervix. Interestingly, axial contractility increased ($p<0.001$) compared to circumferential contractility for all axial-extensions and pressures **(Fig. 7C)**. However, in the passive state, circumferential stress and stiffness increased ($p<0.01$) compared to axial stress and stiffness at matching pressures and axial-extensions **(Fig. 7F)**. Further, circumferential contractility decreased with increasing pressure, yet, axial force with contraction did not change with increasing pressure **(Fig. 6)**. Moreover, axial active stress contributed 54.7±9.19% to the total axial stress while circumferential active stress only contributed 35.0±6.09% to the total circumferential stress. This may suggest a predominant role of axial SMC to resist loading in the axial direction whereas circumferentially aligned collagen within the cervix may function to resist circumferential loading[10, 55, 59]. Supplementing contractility and passive biomechanical data, immunofluorescent imaging demonstrated populations of cSMCs (αSMA^+ cells) within the mid-stroma in both the circumferential and axial planes **(Fig. 8)**. cSMC populations existed only within the mid-stroma suggesting the stroma to be the primary active component of the cervix. Remodeling of ECM and cSMCs within this region may be critical to maintain normal function during pregnancy[16, 48, 55]. Further, analysis identified a larger area fraction of cSMCs within the longitudinal mid-stroma compared to the transverse sections. A larger population of axially aligned cSMCs may prescribe the increased axial contractility within the murine cervix. However, due to the small change in percentage between transverse and longitudinal sections there may be additional cellular mechanisms contributing to axial contractility. Furthermore, rat vaginal tissue under

biaxial loading exhibited a stronger axial contraction in the presence of KCl, however, electrical field stimulation induced increased circumferential contractility [29]. The exact biological mechanisms driving contractility and normal cSMC pacemaker activity within the cervix remain relatively understudied and further investigation into the cholinergic nervous stimulation for cSMC with respect to direction is needed [23].

Cervical insufficiency (CI), a condition in pregnancy in which the cervix prematurely shortens and dilates releasing the uterine contents in the absence of contractions, remains a challenge to diagnose and treat clinically[17, 32, 37]. Prior CI research investigated the role of changing extracellular matrix (ECM) constituents and mechanical loading as potential factors of CI[18, 31, 32, 53]. Interestingly, elastic fiber integrity and content decreases in cases of CI suggesting altered ECM integrity during pregnancy may lead to cervical failure[32]. However, the role of cervical SMC and SMC-ECM interactions remains unknown. Potentially, a loss of axial SMC contractility in response to maladaptive ECM remodeling may result in cervical shortening and dilation characteristic of cervical insufficiency [32, 51]. Future research in pregnancy to describe the dynamic passive biomechanical and contractile behavior of the cervix is needed. The customized methodology described in the current study sets a foundation for future studies in which to explore contraction potential in the cervix through normal pregnancy.

Prior research on the mechanical properties of the murine cervix in uniaxial tension reported similar values of circumferential stiffness (229.74±133.20 kPa/mm) to the values calculated herein (307±133 kPa)[55]. Compared to biaxial active and passive data from the murine vagina, the cervix exhibited similar anisotropic behavior and increased axial contractility. Cervical circumferential stiffness and axial contractility increased compared

414 to the murine vagina in the biaxial inflation-extension configuration[9]. Interestingly, while
415 cervical circumferential stiffness exceeded vaginal measurements, vaginal and cervical
416 axial stiffness were similar in magnitude. Similarly, increased axial contractility with KCl
417 dose was observed in the rat and mouse vagina [9, 29]. Further, the anisotropic behavior of
418 the passive murine cervix with a preference for the circumferential loading direction was
419 observed in the rat and murine vagina and the murine uterus [9, 10, 29].

420 The study did not evaluate potential changes in cervical contractility and passive
421 biomechanics throughout the estrus cycle. However, samples were evaluated at a single
422 stage of the 5-day cycle (estrus) to prevent variability in results. Further, Gravina *et al.*
423 determined the highest contractile potential of the murine cervix at estrus and metestrus[22].
424 Additionally, pilot studies of the passive biomechanics of the murine cervix and uterus
425 revealed no significant differences with estrous phase[10]. The inclusion of the lower uterine
426 and upper vaginal segments may introduce variability into the results. To reduce
427 variability, we tied silk suture over the vaginal and uterine segments during cannulation
428 to prevent contribution to cervical contractility. The dosage of 20 mM diminished
429 contribution of the vaginal segment as the rodent vagina responds to doses greater than
430 30 mM and optimally at 40 mM with tonic contractions[3, 9]. This study assumed
431 conservation of volume, incompressibility, of the cervix in the active and passive
432 protocols, respectively. The estrus cervix may be compressible and the tissue swelled
433 throughout the experiment as glycosaminoglycans sequestered water resulting in a larger
434 passive diameter[11]. However, cervical thickness could not be tracked real-time
435 throughout the experiment due the thickness of the cervical wall preventing light
436 penetration through the tissue and prolonged compression from the ultrasound

transducer resulted in a loss of contractility. Further investigation on isochoric motion during biaxial mechanical testing of the reproductive organs is needed [9, 36].

In summary, the study introduced methods to determine *in vivo* cervical pressure loading environment and apply the *in vivo* pressure to design a protocol to assess biaxial maximum contractility and passive biomechanics of the murine cervix. Determining relationships between cervical SMC contractility and passive function will provide critical information to develop fundamental understanding of physiological cervical function. Further, applying the methods herein throughout pregnancy may provide crucial data about normal remodeling and provide clinically relevant insights into potential mechanisms by which the cervix fails in premature birth induced by cervical insufficiency.

Acknowledgements

The authors wish to thank Gabrielle L. Clark-Patterson, ShanmugaPriyaa Madhukaran, Dylan J. Lawrence, and Carolyn L. Bayer for technical assistance and support.

Funding

This work was supported by NIH R01-HD088481 (MM), NSF CMMI 1751050 (KSM), and the Louisiana Board of Regents Support Fund Fellowship (CKC).

Conflicts of Interest

None to be declared.

References

1. Agianniotis A., A. Rachev and N. Stergiopulos. Active axial stress in mouse aorta. *Journal of Biomechanics* 45: 1924-1927, 2012.

2. Akintunde A., K. M. Robison, D. Capone, L. Desrosiers, L. R. Knoepp and K. S. Miller. Effects of elastase digestion on the murine vaginal wall biaxial mechanical response. *Journal of biomechanical engineering* 2018.

3. Barone W. R., Z. Allah, P. M. Mollie and S. D. Abramowitch. Effect of Active Smooth Muscle Contraction on the Planar Biaxial Mechanical Properties of the Rat Vagina. In: *Midwest American Society of Biomechanics Regional Meeting*. Akron, OH. February 16-17th, 2015: 2015.

4. Barone W. R., A. J. Feola, P. A. Moalli and S. D. Abramowitch. THE EFFECT OF PREGNANCY AND POSTPARTUM RECOVERY ON THE VISCOELASTIC BEHAVIOR OF THE RAT CERVIX. *J Mech Med Biol* 12: 12500091-125000917, 2012.

5. Bersi M., J. Ferruzzi, J. Eberth, R. Gleason and J. Humphrey. Consistent Biomechanical Phenotyping of Common Carotid Arteries from Seven Genetic, Pharmacological, and Surgical Mouse Models. *The Journal of the Biomedical Engineering Society* 42: 1207-1223, 2014.

6. Bulletti C., D. de Ziegler, V. Polli, L. Diotallevi, E. Del Ferro and C. Flamigni. Uterine contractility during the menstrual cycle. *Hum. Reprod.* 15: 81-89, 2000.

7. Byers S. L., M. V. Wiles, S. L. Dunn and R. A. Taft. Mouse estrous cycle identification tool and images. *PloS one* 7: e35538, 2012.

8. Caulk A. W., J. D. Humphrey and S.-I. Murtada. Fundamental Roles of Axial Stretch in Isometric and Isobaric Evaluations of Vascular Contractility. *Journal of biomechanical engineering* 141: 2019.

9. Clark G. L., A. P. Pokutta-Paskaleva, D. J. Lawrence, S. H. Lindsey, L. Desrosiers, L. R. Knoepp, C. L. Bayer, R. L. Gleason and K. S. Miller. Smooth muscle regional contribution to vaginal wall function. *Interface focus* 9: 20190025, 2019.

10. Conway C. K., H. J. Qureshi, V. L. Morris, E. K. Danso, L. Desrosiers, L. R. Knoepp, C. J. Goergen and K. S. Miller. Biaxial biomechanical properties of the nonpregnant murine cervix and uterus. *Journal of Biomechanics* 94: 2019.

11. Cubas J. J. M., R. S. Simões, R. M. Oliveira-Filho, M. J. Simões, E. C. Baracat and J. M. Soares-Jr. Glycosaminoglycan distribution in the rat uterine cervix during the estrous cycle. *Clinics* 65: 703-708, 2010.

12. Danforth D. N. The fibrous nature of the human cervix, and its relation to the isthmic segment in gravid and nongravid uteri. *American Journal of Obstetrics and Gynecology* 53: 541-560, 1947.

13. Darios E. S., B. Seitz and S. W. Watts. Smooth muscle pharmacology in the isolated virgin and pregnant rat uterus and cervix. *The Journal of pharmacology and experimental therapeutics* 341: 587, 2012.

14. de Ziegler D., C. Bulletti, R. Fanchin, M. Epiney and P. A. Brioschi. Contractility of the nonpregnant uterus: the follicular phase. *Annals of the New York Academy of Sciences* 943: 172, 2001.

15. Feola A., P. Moalli, M. Alperin, R. Duerr, R. E. Gandley and S. Abramowitch. Impact of pregnancy and vaginal delivery on the passive and active mechanics of the rat vagina. *Ann Biomed Eng* 39: 549-558, 2011.

16. Ferland D. J., E. S. Darios and S. W. Watts. The persistence of active smooth muscle in the female rat cervix through pregnancy. *American Journal of Obstetrics and Gynecology* 212: 244.e241-244.e248, 2015.

17. Fernandez M. Direct measurement of the permeability of human cervical tissue. *Journal of biomechanical engineering* 135: 021024, 2013.

18. Fernandez M., M. House, S. Jambawalikar, N. Zork, J. Vink, R. Wapner and K. Myers. Investigating the mechanical function of the cervix during pregnancy using finite element models derived from high-resolution 3D MRI. *Computer Methods in Biomechanics and Biomedical Engineering* 19: 404-417, 2016.

19. Ferruzzi J., M. Bersi and J. Humphrey. Biomechanical Phenotyping of Central Arteries in Health and Disease: Advantages of and Methods for Murine Models. *Ann Biomed Eng* 41: 1311-1330, 2013.

20. Ferruzzi J., M. J. Collins, A. T. Yeh and J. D. Humphrey. Mechanical assessment of elastin integrity in fibrillin-1-deficient carotid arteries: implications for Marfan syndrome. *Cardiovascular Research* 92: 287-295, 2011.

21. Gleason R. L., S. P. Gray, E. Wilson and J. D. Humphrey. A Multiaxial Computer-Controlled Organ Culture and Biomechanical Device for Mouse Carotid Arteries. *Journal of biomechanical engineering* 126: 787, 2004.

22. Gravina F. S., D. F. van Helden, K. P. Kerr, R. B. de Oliveira and P. Jobling. Phasic contractions of the mouse vagina and cervix at different phases of the estrus cycle and during late pregnancy. *PLoS One* 9: e111307, 2014.

23. Gravina F. S., D. F. van Helden, K. P. Kerr, R. B. de Oliveira and P. Jobling. Phasic Contractions of the Mouse Vagina and Cervix at Different Phases of the Estrus Cycle and during Late Pregnancy.(Research Article). *PLoS ONE* 9: 2014.

24. Harkness M. L. and R. D. Harkness. Changes in the physical properties of the uterine cervix of the rat during pregnancy. *The Journal of physiology* 148: 524, 1959.

25. Harkness M. L. and R. D. Harkness. The mechanical properties of the uterine cervix of the rat during involution after parturition. *The Journal of physiology* 156: 112, 1961.

26. Harkness R. D. and B. E. Moralee. The time- course and route of loss of collagen from the rat's uterus during post- partum involution. *The Journal of physiology* 132: 502, 1956.

27. Herington J. L., C. O'Brien, M. F. Robuck, W. Lei, N. Brown, J. C. Slaughter, B. C. Paria, A. Mahadevan-Jansen and J. Reese. Prostaglandin- Endoperoxide Synthase 1 Mediates the Timing of Parturition in Mice Despite Unhindered Uterine Contractility. *Endocrinology* 159: 490, 2018.

28. Humphrey J. D. *Cardiovascular Solid Mechanics Cells Tissues and Organs*. New York: Springer-Verlag New York Inc., 2002.

29. Huntington A., E. Rizzuto, S. Abramowitch, Z. Del Prete and R. De Vita. Anisotropy of the Passive and Active Rat Vagina Under Biaxial Loading. *Annals of Biomedical Engineering* 2018.

30. Huo Y., Y. Cheng, X. Zhao, X. Lu and G. S. Kassab. Biaxial vasoactivity of porcine coronary artery. *American journal of physiology. Heart and circulatory physiology* 302: H2058, 2012.

31. Leppert P. C., J. M. Cerreta and I. Mandl. Orientation of elastic fibers in the human cervix. *American Journal of Obstetrics and Gynecology* 155: 219, 1986.

32. Leppert P. C., S. Y. Yu, S. Keller, J. Cerreta and I. Mandl. Decreased elastic fibers and desmosine content in incompetent cervix. *American Journal of Obstetrics and Gynecology* 157: 1134, 1987.

33. Lowder J. L., K. M. Debes, D. K. Moon, N. Howden, S. D. Abramowitch and P. A. Moalli. Biomechanical adaptations of the rat vagina and supportive tissues in pregnancy to accommodate delivery. *Obstet Gynecol* 109: 136-143, 2007.

34. Manoogian S. J., C. McNally, J. D. Stitzel and S. M. Duma. Dynamic biaxial tissue properties of pregnant porcine uterine tissue. *Stapp car crash journal* 52: 167, 2008.

35. Milsom I., B. Andersch and G. Sundell. The Effect Of Flurbiprofen And Naproxen Sodium On Intra-Uterine Pressure And Menstrual Pain In Patients With Primary Dysmenorrhea. *Acta Obstetricia et Gynecologica Scandinavica* 67: 711-716, 1988.

36. Murtada S.-I., J. Ferruzzi, H. Yanagisawa and J. Humphrey. Reduced Biaxial Contractility in the Descending Thoracic Aorta of Fibulin-5 Deficient Mice. *Journal of biomechanical engineering* 138: 051008, 2016.

37. Myers K. M., H. Feltovich, E. Mazza, J. Vink, M. Bajka, R. J. Wapner, T. J. Hall and M. House. The mechanical role of the cervix in pregnancy. *Journal of Biomechanics* 48: 1511-1523, 2015.

38. Myers K. M., S. Socrate, A. Paskaleva and M. House. A study of the anisotropy and tension/compression behavior of human cervical tissue. *Journal of biomechanical engineering* 132: 021003, 2010.

39. Nallasamy S. and M. Mahendroo. Distinct Roles of Cervical Epithelia and Stroma in Pregnancy and Parturition. 35: 190-200, 2017.

40. Omari E. A., T. Varghese, M. A. Kliewer, J. Harter and E. M. Hartenbach. Dynamic and quasi- static mechanical testing for characterization of the viscoelastic properties of human uterine tissue. *Journal of Biomechanics* 48: 1730-1736, 2015.

41. Pearsall G. W. and V. L. Roberts. Passive mechanical properties of uterine muscle (myometrium) tested in vitro. *Journal of Biomechanics* 11: 167,173-171,176, 1978.

42. Robison K. M., C. K. Conway, L. Desrosiers, L. R. Knoepp and K. S. Miller. Biaxial Mechanical Assessment of the Murine Vaginal Wall Using Extension-Inflation Testing. *Journal of biomechanical engineering* 139: 2017.

43. Robuck M. F., C. M. O'Brien, K. M. Knapp, S. D. Shay, J. D. West, J. M. Newton, J. C. Slaughter, B. C. Paria, J. Reese and J. L. Herington. Monitoring uterine contractility in mice using a transcervical intrauterine pressure catheter. *Reproduction (Cambridge, England)* 155: 447, 2018.

44. Sokolis D. P. Experimental investigation and constitutive modeling of the 3D histomechanical properties of vein tissue. *Biomechanics and modeling in mechanobiology* 12: 431-451, 2013.

45. Sokolis D. P. Strain-energy function and three-dimensional stress distribution in esophageal biomechanics. *Journal of Biomechanics* 43: 2753-2764, 2010.

46. Stavropoulou E. A., Y. F. Dafalias and D. P. Sokolis. Biomechanical behavior and histological organization of the three-layered passive esophagus as a function of topography. *Proceedings of the Institution of Mechanical Engineers, Part H: Journal of Engineering in Medicine* 226: 477-490, 2012.

47. Stoka K. V., J. A. Maedeker, L. Bennett, S. A. Bhayani, W. S. Gardner, J. D. Procknow, A. J. Cocciolone, T. A. Walji, C. S. Craft and J. E. Wagenseil. Effects of Increased Arterial Stiffness on Atherosclerotic Plaque Amounts. *Journal of biomechanical engineering* 140: 2018.

48. Tantengco O. A. G. and R. Menon. Contractile function of the cervix plays a role in normal and pathological pregnancy and parturition. *Medical hypotheses* 145: 2020.

49. Toner J. P. and N. T. Adler. The role of uterine luminal fluid in uterine contractions, sperm transport and fertility of rats. *Journal of Reproduction and Fertility* 74: 295-302, 1985.

50. Van Loon P. Length-force and volume-pressure relationships of arteries. *Biorheology* 14: 181-201, 1976.

51. Vink J., V. Yu, S. Dahal, J. Lohner, C. Stern-Asher, M. Mourad, G. Davis, Z. Xue, S. Wang, K. Myers, J. Kitajewski, X. Chen, R. J. Wapner, C. V. Ananth, M. Sheetz and G. Gallos. Extracellular Matrix Rigidity Modulates Human Cervical Smooth Muscle Contractility-New Insights into Premature Cervical Failure and Spontaneous Preterm Birth. *Reproductive sciences (Thousand Oaks, Calif.)* 2020.

52. Vink J. Y., S. Qin, C. O. Brock, N. M. Zork, H. M. Feltovich, X. Chen, P. Urie, K. M. Myers, T. J. Hall, R. Wapner, J. K. Kitajewski, C. J. Shawber and G. Gallos. A new

paradigm for the role of smooth muscle cells in the human cervix. *American Journal of Obstetrics and Gynecology* 2016.

53. Westervelt A. R., M. Fernandez, M. House, J. Vink, C.-L. Nhan-Chang, R. Wapner and K. M. Myers. A Parameterized Ultrasound-Based Finite Element Analysis of the Mechanical Environment of Pregnancy. *Journal of biomechanical engineering* 139: 2017.

54. White S. E., C. K. Conway, G. L. Clark, D. J. Lawrence, C. L. Bayer and K. S. Miller. Biaxial Basal Tone and Passive Testing of the Murine Reproductive System Using a Pressure Myograph. *Jove-Journal of Visualized Experiments* 2019.

55. Yoshida K., H. Jiang, M. Kim, J. Vink, S. Cremers, D. Paik, R. Wapner, M. Mahendroo and K. Myers. Quantitative evaluation of collagen crosslinks and corresponding tensile mechanical properties in mouse cervical tissue during normal pregnancy. *PLoS ONE* 9: e112391, 2014.

56. Yoshida K., M. Mahendroo, J. Vink, R. Wapner and K. Myers. Material properties of mouse cervical tissue in normal gestation. *Acta Biomaterialia* 36: 195-209, 2016.

57. Yoshii A., S. Kitahara, H. Ueta, K. Matsuno and T. Ezaki. Role of Uterine Contraction in Regeneration of the Murine Postpartum Endometrium 1. *Biology of Reproduction* 91: 2014.

58. Zhou B., A. Rachev and T. Shazly. The biaxial active mechanical properties of the porcine primary renal artery. *Journal of the Mechanical Behavior of Biomedical Materials* 48: 28-37, 2015.

59. Zork N. M., K. M. Myers, K. Yoshida, S. Cremers, H. Jiang, C. V. Ananth, R. J. Wapner, J. Kitajewski and J. Vink. A systematic evaluation of collagen cross-links in the

635 human cervix. *American Journal of Obstetrics and Gynecology* 212: 321.e321-
636 321.e328, 2015.

637

638

Figures and Tables:

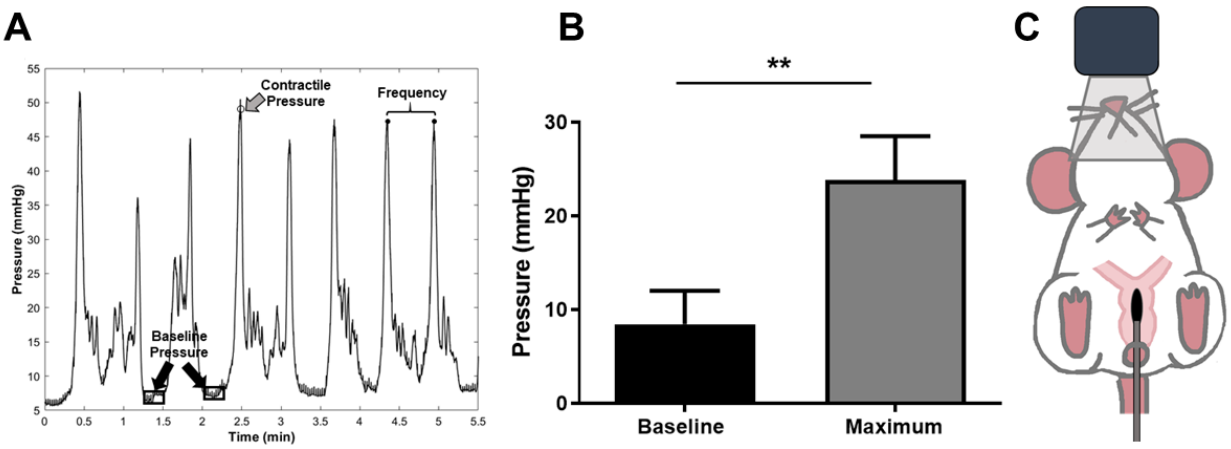

Figure 1: (A) Representative recording of *in vivo* pressure measurements utilizing ADInstruments Labchart software. *In vivo* cervical smooth muscle behavior exhibited a phasic response characterized by regular contractions throughout the recording. Average pressure between contractions, at the troughs of the waves, determined baseline pressure (black arrows and box). Contractile pressure (gray arrow and open circle) were taken at the peaks to determine average contracted pressure. Time from peak to peak determined the frequency (black closed circles) of contractions for each data set. **(B)** Average *in vivo* baseline (black) and maximum contractile (gray) pressure measurements in nulliparous mice at estrus (n=5). ADInstruments Labchart software determined the average baseline (P= 9.00±3.00 mmHg) and maximum (P= 22.0±4.00 mmHg) pressures. Pressure increased significantly (*p<0.01; ***) from the baseline to maximum amplitude during contraction. **(C)** Graphic representing the catheter placement within the cervix *in vivo* during data collection.

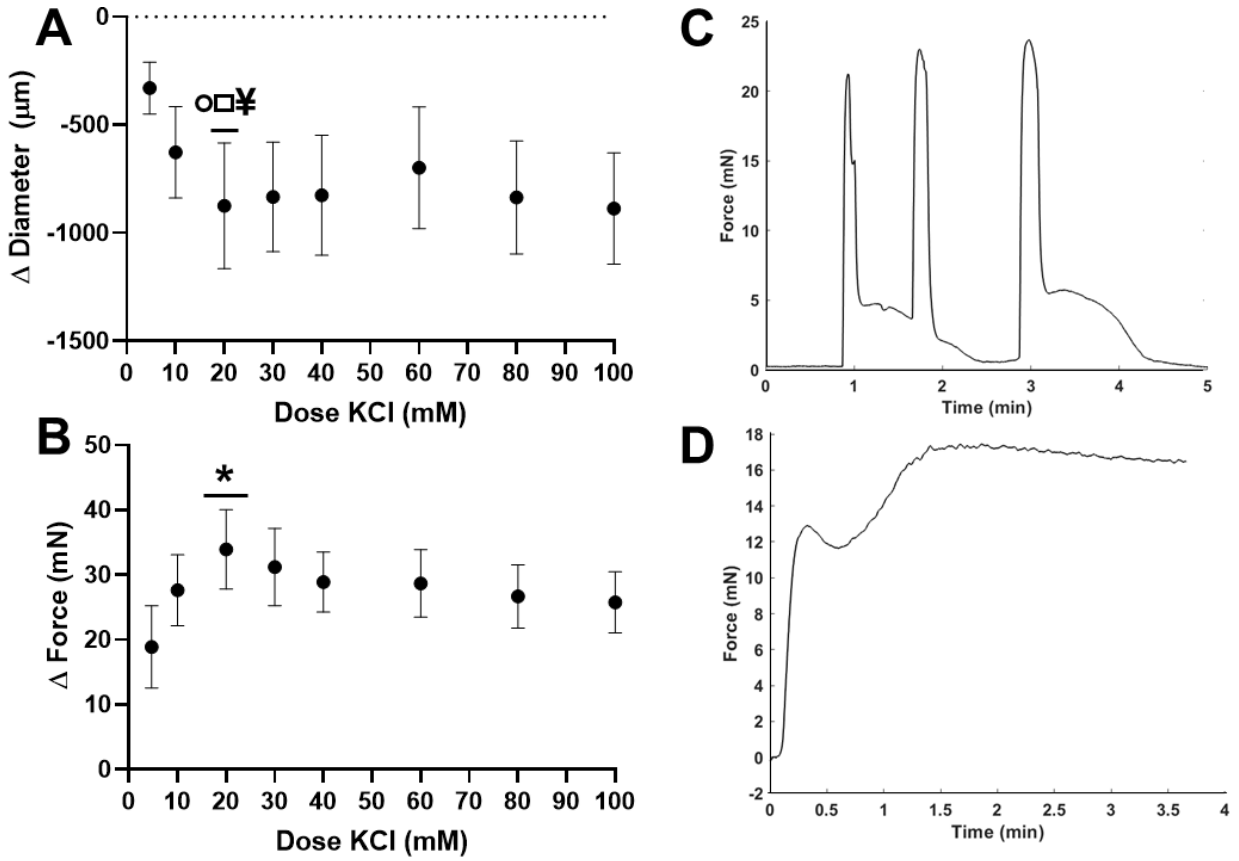

Figure 2: KCl dose response circumferential **(A)** and axial **(B)** contractility results with respect to the estimated physiologic (EP) length and mean physiologic pressure. **(A)** Change in diameter with contraction decreased from 4.7-20 mM KCl (*p<0.05;* 4.7 circle; 10 square) compared to 20mM and plateaued from 20-100mM. However, total change in diameter with contraction at 60mM increased significantly (*p<0.05;* ¥) compared to 20mM. **(B)** Change in force with contraction increased significantly at 20mM compared to all doses *(p<0.05; *).* Further with increasing dose, contractile behavior altered from a phasic **(C)** to tonic **(D)** pattern as shown in the representative sample for 20mM **(C)** and 60 mM **(D)**. Phasic contractile behavior persisted through 20mM KCl **(C)**, and doses 40-100mM exhibited tonic contractile behavior resulting in plateaued force and outer diameter. Frequency of contractions increased non-significantly from the baseline concentration

669 (4.7mM; 0.03±0.02Hz) up to 0.05±0.02 Hz at 20mM. Following 40 mM of KCl, the
670 concentration frequency decreased to 0Hz with tonic contraction.
671
672

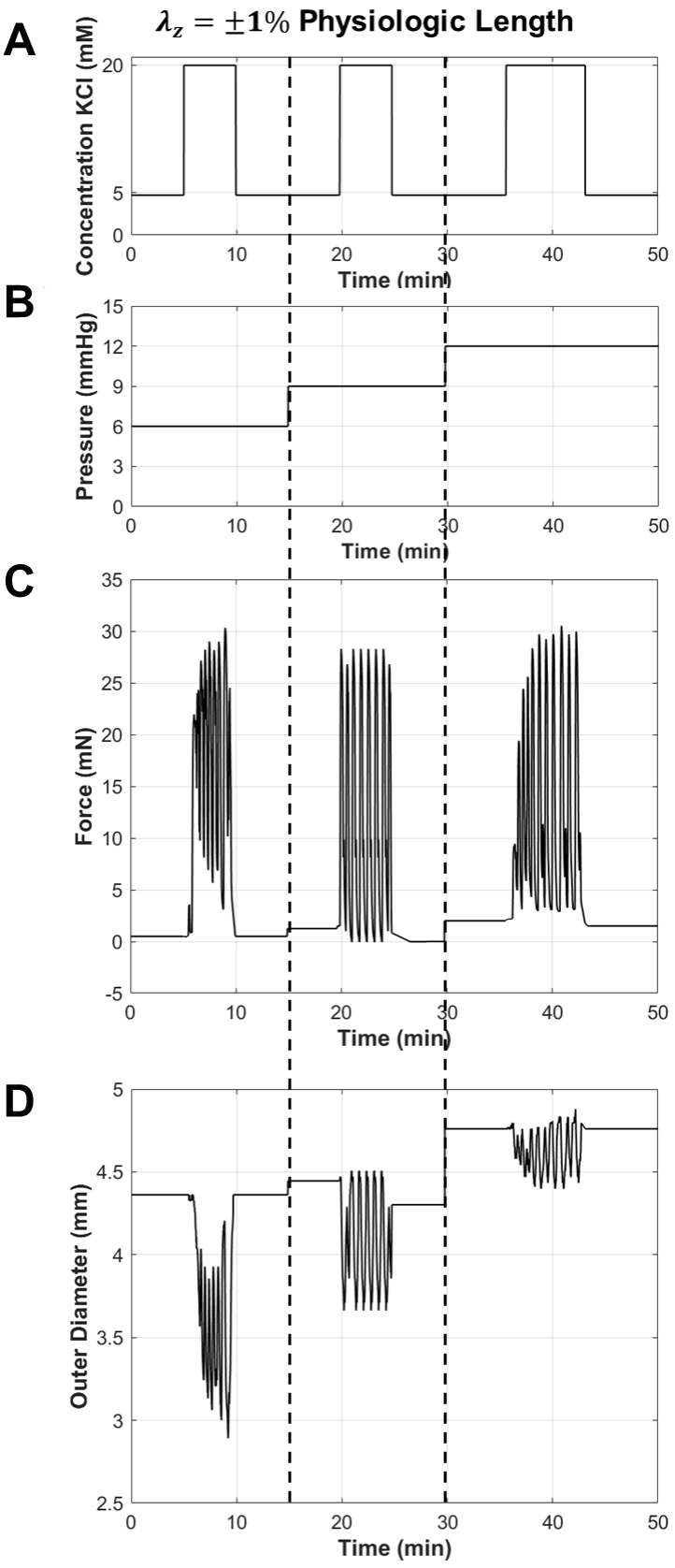

Figure 3: Maximum contractility testing protocol schematic for set axial-extension and alternating pressures. Cervices equilibrated after each test for five minutes followed by five minutes of equilibration with each change in pressure or axial-extension. **(A)** Times and concentrations of KCl within the tissue bath. Wherein 20 mM induced maximum contraction and 4.7 mM acted as the baseline content in Kreb's solution. **(B)** Pressure throughout maximum contractility testing for one axial-extension. Maximum contractility was induced at the mean physiologic pressure (P= 9.0±3.0 mmHg). Dashed lines represent the pressure change throughout the protocol. **(C, D)** Change in force and outer diameter with maximum contraction and during equilibration periods.

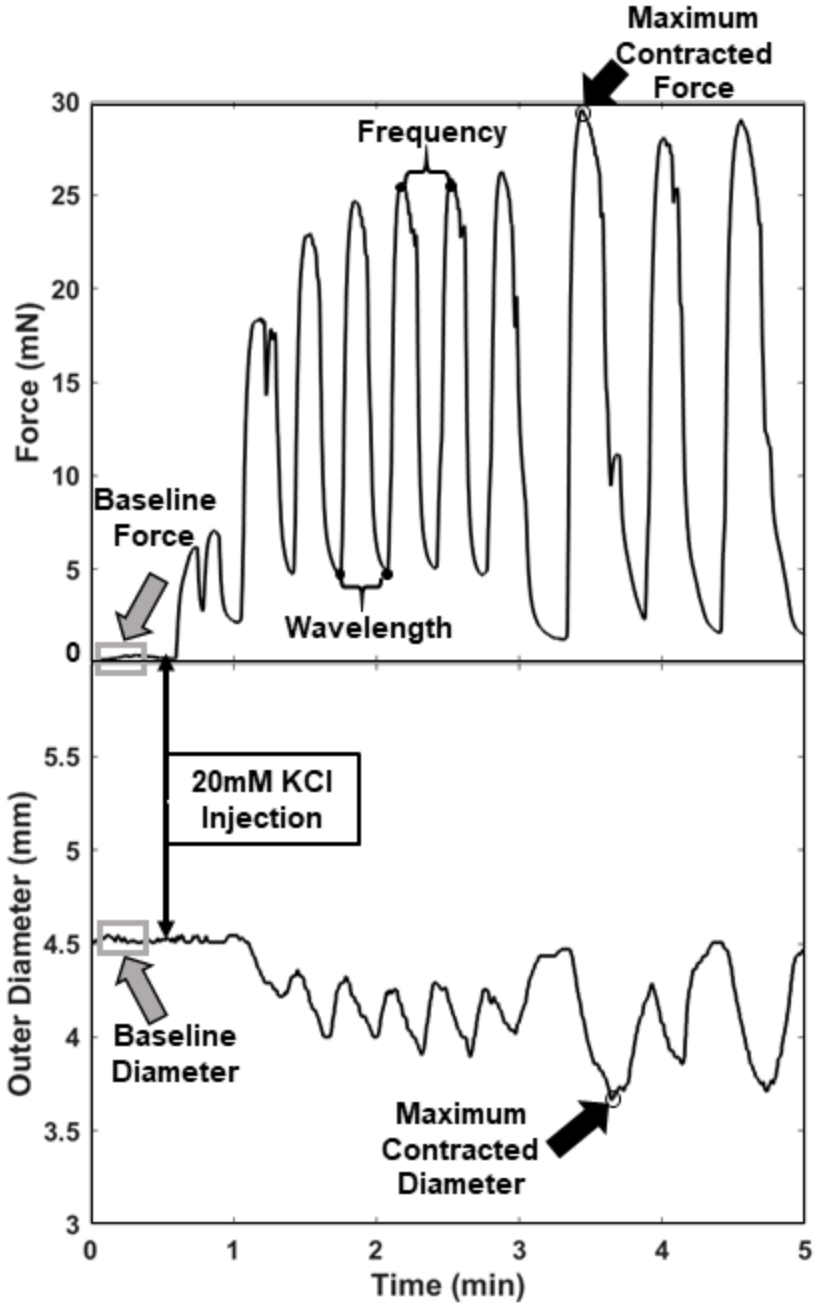

Figure 4: Representative schematic of testing data from a maximum contractility test executed at the estimated physiologic (EP) length and mean physiologic pressure. Baseline force and diameter (gray arrows and boxes) were recorded at the beginning of the test prior to KCl injection. Wavelength (closed circles at troughs) was measured as the time for a contraction to complete one cycle (trough to trough). Whereas frequency (closed circles at peak) was measured as the number of contractions within a time frame (peak to peak). Maximum contracted force and diameter (black arrows and open circles) were identified as the maximal force at the inflection of a contraction and the corresponding diameter.

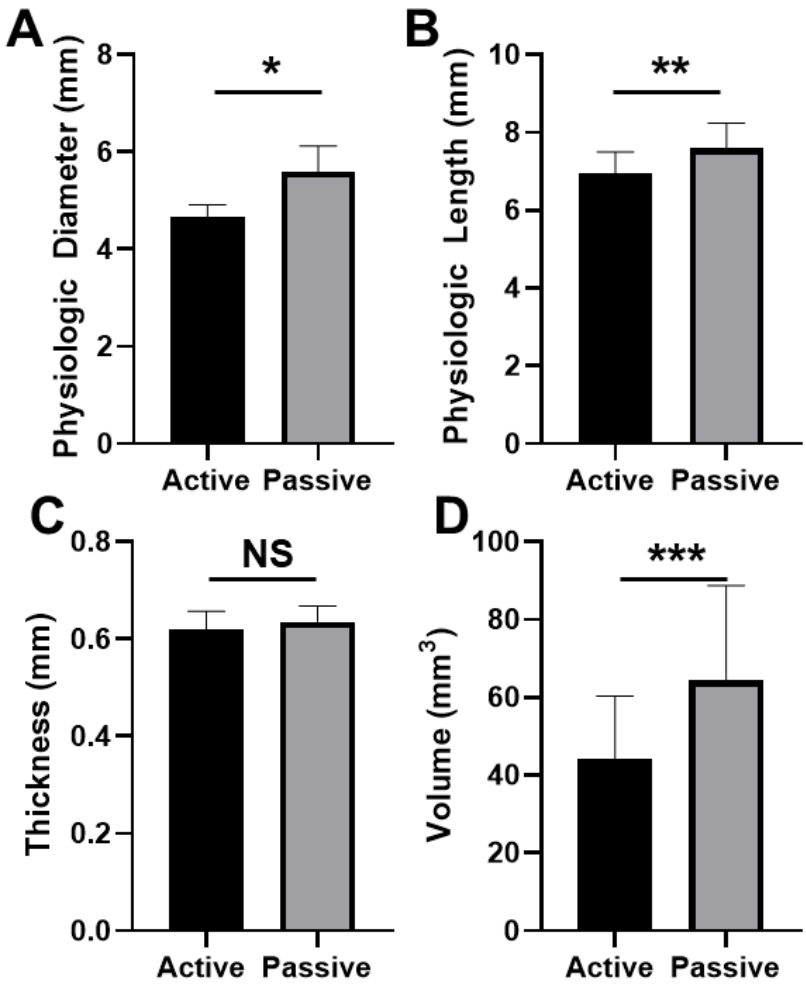

Figure 5: Geometry recorded during mechanical testing at the active (black) and passive (gray) states revealed a significant increase in passive geometry. **(A)** Physiologic diameter, the diameter at the physiologic length and mean physiologic pressure, increased significantly (*p<0.05; **) from 4.67±0.25 mm to 5.59±0.53 mm. **(B)** Physiologic length significantly increased *(p<0.01; ***) from 6.96±0.54 mm to 7.59±0.66 mm between active and passive protocols. **(C)** Thickness did not significantly increase in the passive state (0.62±0.04 mm vs 0.64±0.03 mm). **(D)** Volume of the unloaded cervix increased significantly (*p<0.005;****) after smooth muscle relaxation where the active volume measured 44.2±7.22 mm^3 and the passive measured at 64.3±11.0 mm^3.

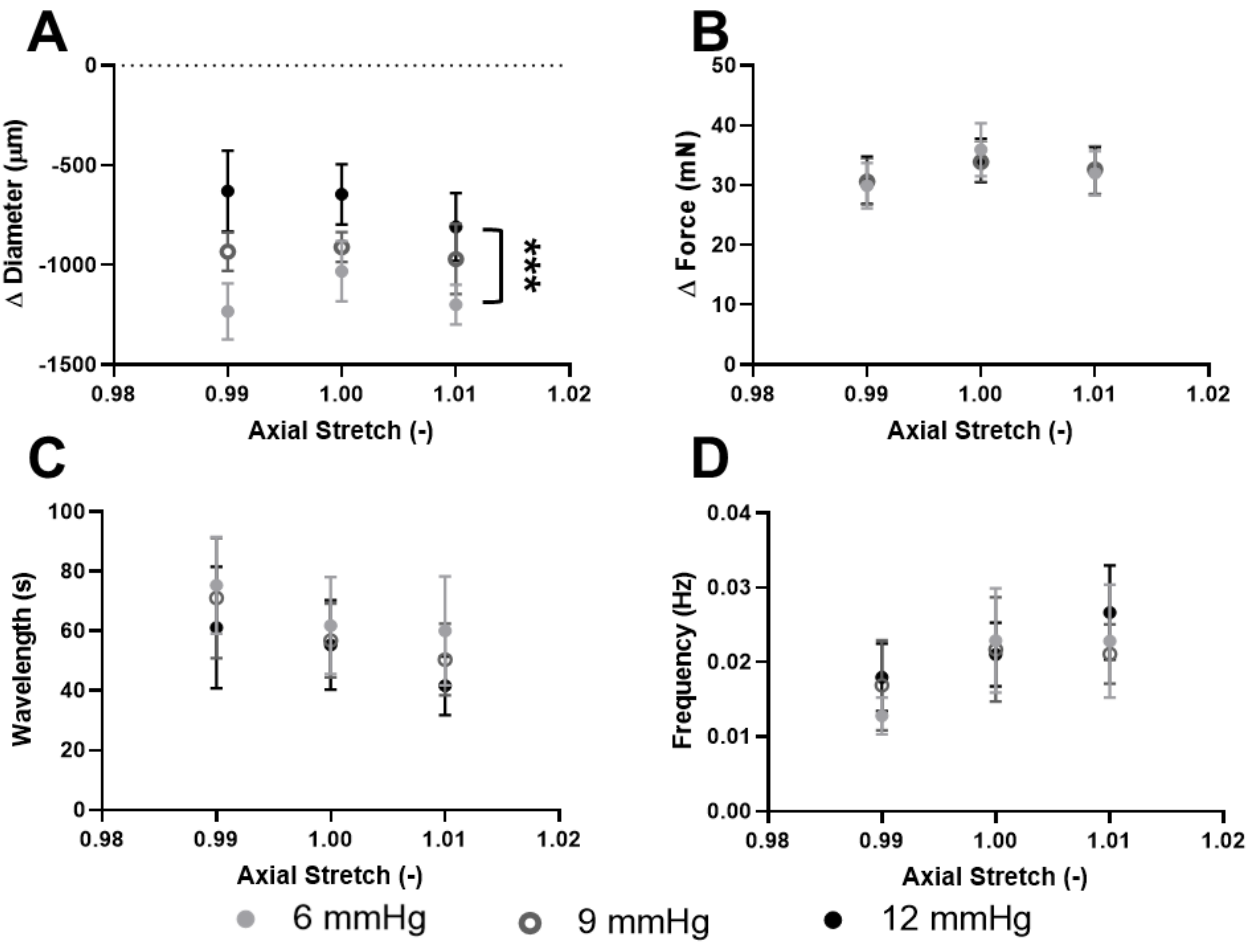

Figure 6: (A) Circumferential contraction measured by change in diameter during maximum contractility protocol at 9 combinations of pressures (P=9.0±3.0 mmHg) and axial-extensions ±1% EPL (*n=5*). Where 6 mmHg is represented by gray closed circles, 9 mmHg by dark gray open circles, and 12 mmHg as black closed circles. Total change in diameter during contraction significantly decreased (*p<0.001;* ***) at the high pressure (P= 12 mmHg; black closed) compared to the low pressure (P= 6 mmHg; gray closed) loading for all axial-stretches. **(B)** Axial contraction measured by change in force did not significantly differ with axial-stretch or pressure. **(C, D)** Wavelength and frequency of contractions induced by 20 mM KCl did not significantly differ with increase pressure or axial-stretch.

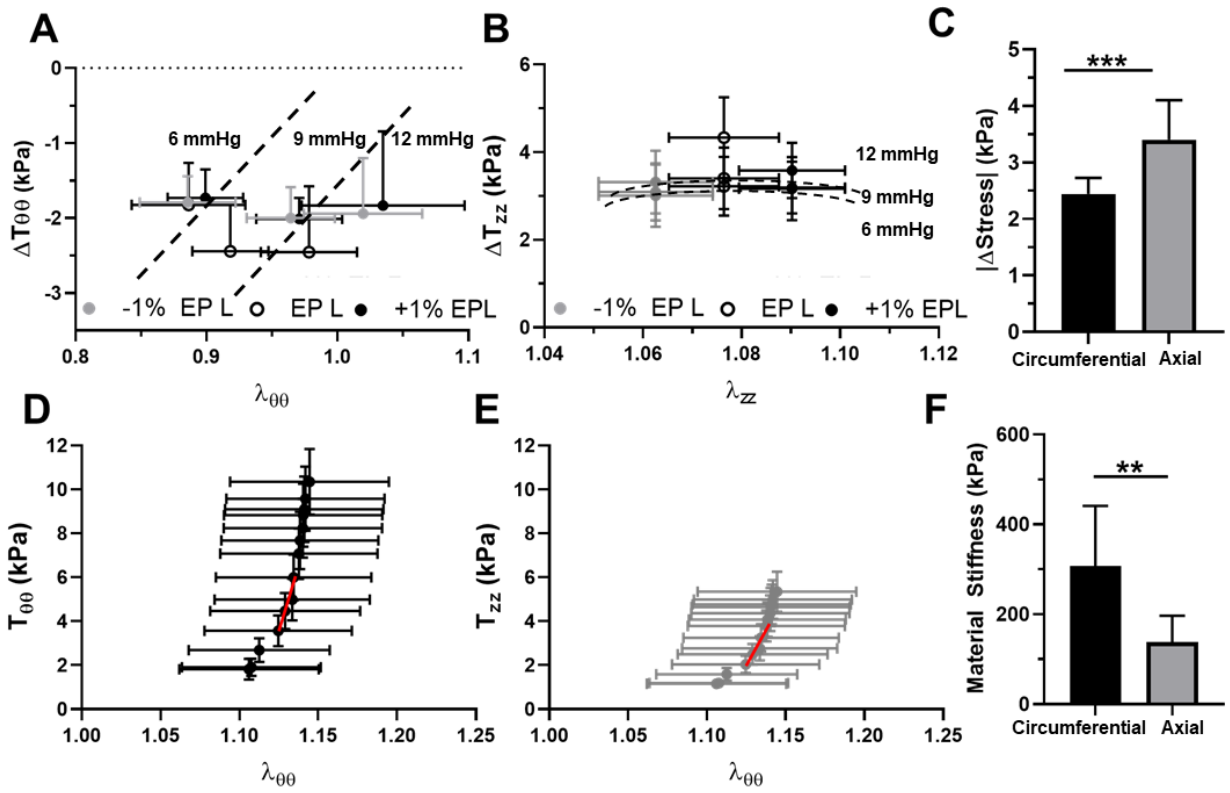

Figure 7: (A) Isolated active mechanical contribution in circumferential stress against circumferential stretch during at the estimated physiologic length (EP L; dark gray open circles), -1% EP L (closed gray circles), and +1% EPL (closed black circles) for all pressures (*n=5*). Stresses within a pressure grouping are separated by dashed lines. **(B)** Isolated active contribution with respect to the axial stress plotted against axial stretch for all axial stretches and pressures. Where dashed lines separate the mean physiologic pressure (P= 9.0 mmHg) from the above (P= 12 mmHg) and below (P= 6.0 mmHg) pressure groupings. **(C)** Absolute change in circumferential (black) and axial (gray) stress at the EP length and pressure where axial stress (3.40±0.70 kPa) significantly (*p<0.001; **)* increased compared to circumferential stress (2.44±0.28 kPa) during maximum contraction. **(D)** Circumferential (black) and **(E)** axial (gray) stress-stretch curves with respect to the circumferential stretch, respectively. The physiologic range of pressures

(P= 9.0±3.0 mmHg) during the passive mechanical test were mapped to corresponding circumferential stretches and stresses. The lines denote the area of the stress-stretch curves in which the slope was determined for material stiffness calculations. **(F)** Circumferential (black) and axial (gray) material stiffness from the EP length. Two-way ANOVA (axial-stretch, direction) and post-hoc t-tests confirmed a significant increase ($p<0.01$) in circumferential stiffness (327± 142 kPa) compared to axial stiffness (136 ± 51.2 kPa).

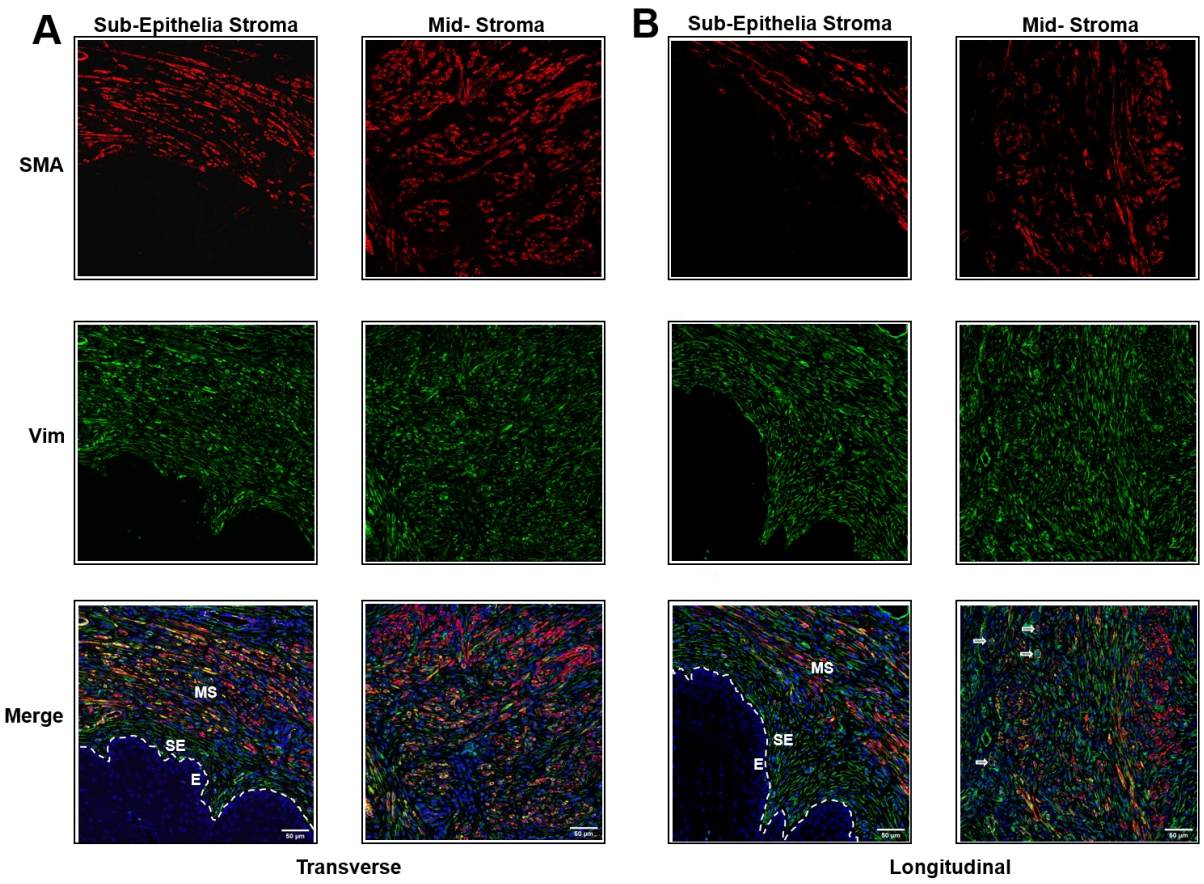

763

764 **Figure 8:** Dual immunofluorescent imaging taken at 20x of **α**SMA$^+$ (SMA, red) and
765 vimentin$^+$ (Vim, green) cells in the **(A)** transverse and **(B)** longitudinal plane of the sub-
766 epithelial stroma (SE) and mid-stroma (MS) from cervical sections taken from mice in
767 estrus (*n=2*). Wherein the αSMA$^+$ cells represent cSMCs, vimentin$^+$ cells represent
768 fibroblasts, cells co-stained with **α**SMA$^+$ and vimentin$^+$ (yellow) indicate myofibroblasts,
769 and arrowheads indicate blood vessels. The SE stroma populations primarily contain
770 vimentin$^+$ cells, while the MS contains both vimentin$^+$ and **α**SMA$^+$ cells. Comparatively,
771 fewer cells in the MS region co-stain for vimentin$^+$ and **α**SMA$^+$.

772 **Supplemental Figures**

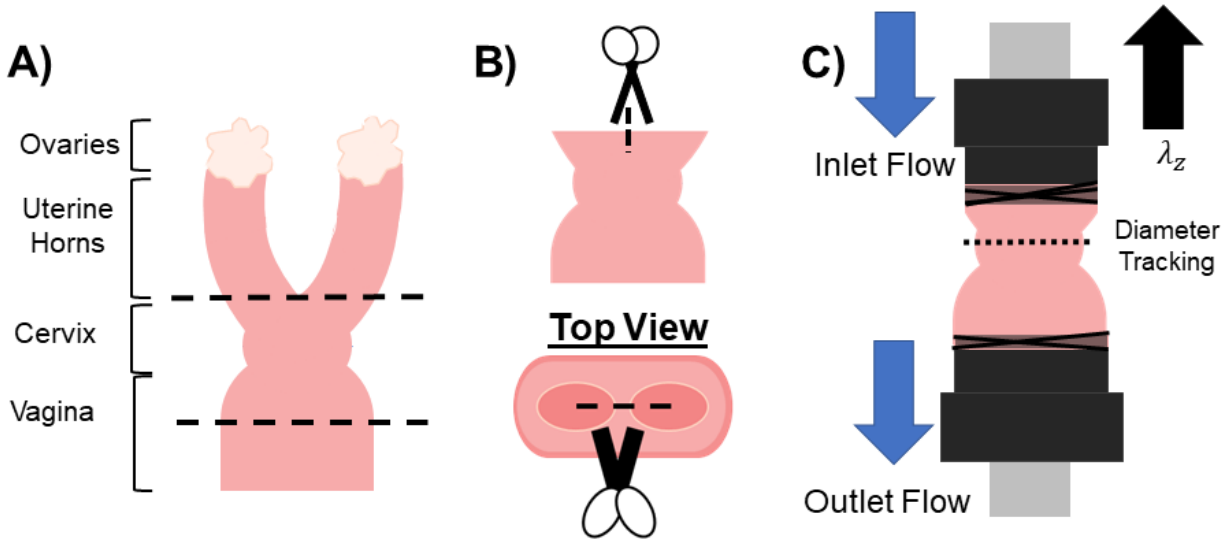

Supplemental Figure 1: (A) Graphic of the murine reproductive tract highlighting the approximate geometry and location of the ovaries, uterine horns, cervix, and vagina. Where the dashed lines represent the location of cuts made during dissection to isolate the cervix. Contrastingly to the human reproductive system, the murine reproductive system includes two uterine horns that meet to form a single canal within the cervix. Prior research of the mouse reproductive tract reports approximate diameter values of 2.0 mm for the uterine horn [1], 3.25 mm for the cervix [1], 6.0 mm for the proximal vagina [2], and 5.5 mm for the distal vagina [2]. **(B)** Graphic outlining specimen preparation of the cervix for cannulation. Due to the short length of the murine cervix, a small portion of uterine horn and vagina remain attached to be used as anchor points within the biaxial device without interfering with cervical geometry. To finalize preparation of the cervix for cannulation, the uterine horns are cut down to the bifurcation point (seen in the top view) and utilizing micro-scissors the wall separating the uterine canals was cut. **(C)** Schematic of the cervix cannulated within the biaxial inflation-extension device. The vaginal and uterine ends were pulled gently onto the cannula and secured with 6-0 silk suture. The Danish Myoview Technology software and an Olympus camera tracked the outer

diameter at the mid-cervix represented by the dashed line. Pressure transducers and a pump controlled the flow and pressure of the Kreb's Ringer Buffer through hollow tubes in the cannula into the tissue. The inlet flow was aligned with the uterine end and the outlet flow with the vaginal end to simulate the flow or labor or menstruation. Simultaneously, a manual axial micrometer controlled the axial length and stretch (λ_z) of the tissue at a rate of 0.01mm/sec.

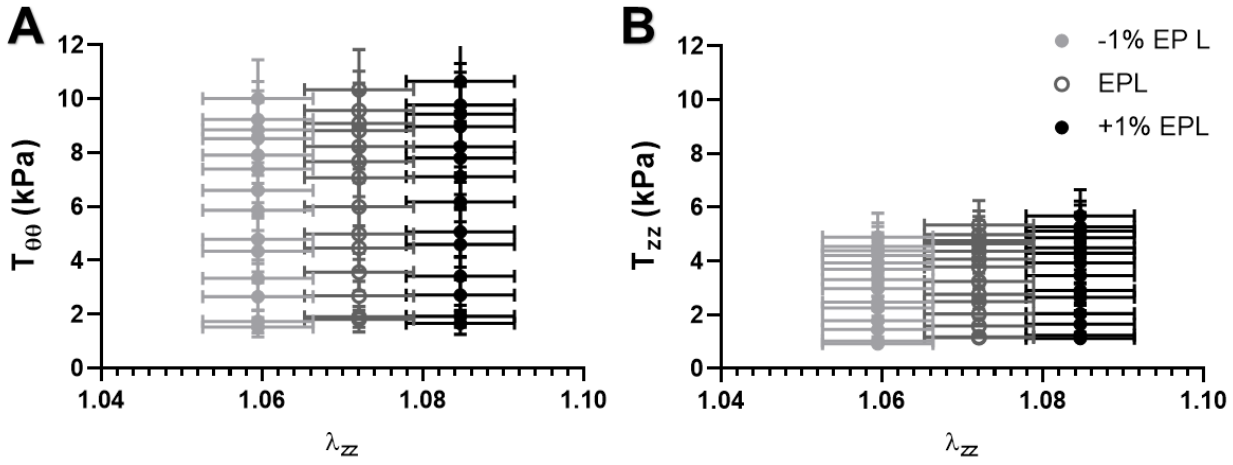

Supplemental Figure 2: (A) Circumferential ($T_{\theta\theta}$) and **(B)** axial (T_{zz}) stress with respect to axial-stretch (λ_{zz}) from the pressure-inflation cycles at the estimated physiologic (EP) length (dark gray open circle), -1% EPL (light gray close circle), and +1% EPL (black closed circle). Neither circumferential nor axial stress changed significantly with axial-stretch.

[1] C.K. Conway, H.J. Qureshi, V.L. Morris, E.K. Danso, L. Desrosiers, L.R. Knoepp, C.J. Goergen, K.S. Miller, Biaxial biomechanical properties of the nonpregnant murine cervix and uterus, Journal of Biomechanics 94 (2019).

[2] G.L. Clark, A.P. Pokutta-Paskaleva, D.J. Lawrence, S.H. Lindsey, L. Desrosiers, L.R. Knoepp, C.L. Bayer, R.L. Gleason, K.S. Miller, Smooth muscle regional contribution to vaginal wall function, Interface focus 9(4) (2019) 20190025.